Inserting Nitrogen: An Effective Concept to Create Non-Planar and Stimuli-Responsive Perylene Bisimide Analogues

Sakiho Hayakawa,[†] Ayumi Kawasaki,[‡,§] Yongseok Hong,[∥] Daisuke Uraguchi,[†] Takashi Ooi,[†,⊥] Dongho Kim,*[,∥] Tomoyuki Akutagawa,*[,‡,§] Norihito Fukui,*[,†] and Hiroshi Shinokubo*[,†]

† Department of Molecular and Macromolecular Chemistry, Graduate School of Engineering, Nagoya University, Furo-cho, Chikusa-ku, Nagoya, Aichi 464-8603, Japan

‡ Graduate School of Engineering, Tohoku University, Sendai 980-8579, Japan

§ Institute of Multidisciplinary Research for Advanced Materials (IMRAM), Tohoku University, 2-1-1 Katahira, Aoba-ku, Sendai 980-8577, Japan

∥ Spectroscopy Laboratory for Functional π-Electronic Systems and Department of Chemistry, Yonsei University, Seoul 03722, Korea

⊥ Institute of Transformative Bio-Molecules (WPI-ITbM), Nagoya University, Furo-cho, Chikusa-ku, Nagoya 464-8601, Japan

ABSTRACT: Establishing design principles to create non-planar π-conjugated molecules is crucial for the development of novel functional materials. Herein, we describe the synthesis and properties of dinaphtho[1,8-bc:1',8'-ef]azepine bisimides (DNABIs). Their molecular design is conceptually based on the insertion of a nitrogen atom into a perylene bisimide core. We have synthesized several DNABI derivatives with a hydrogen atom, a primary alkyl group, or an aryl group on the central nitrogen atom. These DNABIs exhibit non-planar conformations, flexible structural changes, and ambipolar redox activity. The steric effect around the central nitrogen atom substantially affects the overall structures and results in two different conformations: a nonsymmetric bent conformation and a symmetric twisted conformation, accompanied by a drastic change in electronic properties. Notably, the nonsymmetric DNABI undergoes unique structural changes in response to the application of an external electric field, which is due to molecular motions that are accompanied by an orientational fluctuation of the dipole moment. Furthermore, the addition of a chiral Brønsted base to *N*-unsubstituted DNABI affords control over the helical chirality *via* hydrogen-bonding interactions.

INTRODUCTION

Establishing guidelines for the design of non-planar π-conjugated molecules is crucial for the development of novel functional materials.[1−13] Non-planar π-systems exhibit numerous intriguing properties such as three-dimensional conformations, structural flexibility, high solubility, chirality, and specific intermolecular interactions such as concave−convex interactions.[13−30] Manipulating non-planarity represents a strategy that has offered practical applications including high-performance organic semiconductors,[31−34] unique host-guest systems,[35−38] and functional supramolecular assemblies.[39−40] One representative approach to design non-planar π-systems is to incorporate seven-membered ring(s) into a fused π-system. Pioneering work in this area dates back to the synthesis of [7]circulene by Yamamoto and co-workers in 1983,[41,42] and a variety of curved aromatic hydrocarbons has been reported since.[43−57] Among these, the negatively curved nanographene **1** reported by Miao and co-workers is worth noting in light of its molecular design, which is based on inserting a methylene unit into a planar hexa-*peri*-benzocoronene skeleton (Figure 1a).[46] Osuka and co-workers have inserted several atomic units into triply linked porphyrin arrays, yielding so-called porphyrin arch-tapes **2**.[58−60] This strategy should be applicable to a wide range of planar π-conjugated systems in order to create various non-planar molecules. In particular, the insertion of a heteroatom moiety is advantageous due to the peculiar electronic perturbation of the neighboring π-systems and the potential ability to respond to external stimuli.[61,62]

Perylene bisimide (PBI) is an attractive π-conjugated molecule that exhibits exceptional light-harvesting properties, a high fluorescence quantum yield, strong electron-deficiency, and excellent photostability.[63−68] The development of structurally distorted PBI derivatives has been actively explored for the past decade, mostly encouraged by their potential utility as non-fullerene acceptors for organic photovoltaics and chiral optoelectronic materials.[69−79] However, the latest guidelines for the molecular design of non-planar PBI analogues relies on a functionalization at the bay area to induce intramolecular steric repulsion (Figure 1b).

Herein, we disclose a strategy to access the non-planar PBI analogues dinaphtho[1,8-bc:1',8'-ef]azepine bisimides (DNABIs) (Figure 1b). DNABIs exhibit non-planar conformations and ambipolar redox activity. Importantly, the steric effect around the inserted nitrogen atom drastically affects the molecular structure and the electronic properties. Moreover, the resulting DNABIs respond uniquely toward the application of an electric field and to the presence of hydrogen-bond acceptors. It is worth noting that DNABIs are structurally related to dinaphtho[1,8-bc:1',8'-ef]heteropines.[80,81] However, the latter are limited to boron- and oxygen-containing analogues, probably due to the synthetic difficulties associated with

attaching planar naphthalene units around a non-planar seven-membered ring.

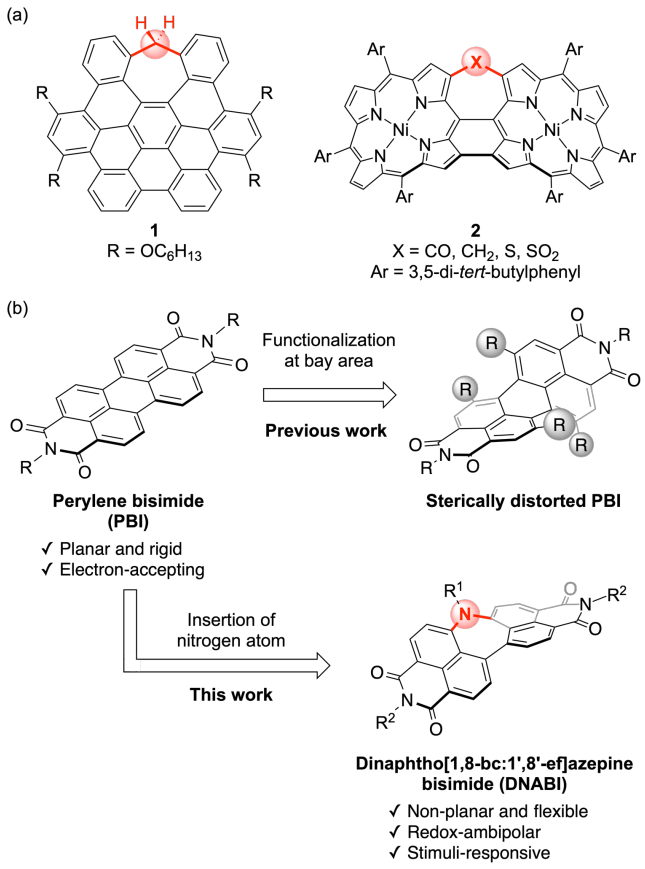

Figure 1. (a) Chemical structures of negatively curved nanographene **1** and porphyrin arch-tape **2**. (b) Design concepts for non-planar PBI analogues.

RESULTS AND DISCUSSION

Synthesis. The synthesis of DNABIs **5**–**8** is shown in Scheme 1. 4-Bromo-5-iodonaphthalene monoimides **3a** and **3b** were synthesized according to literature procedures.[82,83] The intermolecular C–I/C–I homocoupling reaction[84] of **3a** and **3b** using copper(I) 2-thiophenecarboxylate (CuTC) provided the corresponding dimers **4a** and **4b** in 41% and 66% yield, respectively. A Buchwald–Hartwig amination[85,86] of **4a** with octylamine and 4-methoxybenzylamine afforded *N*-octyl DNABI **5a** and *N*-4-methoxybenzyl DNABI **6a** in 44% and 48% yield, respectively. The reaction of **4a** and **4b** with aniline furnished the corresponding *N*-phenyl DNABIs **7a** and **7b** in 11% and 7% yield, respectively. Treatment of **6a** with an excess of anisole and trifluoroacetic acid resulted in the deprotection of the 4-methoxybenzyl group to provide *N*-unsubstituted DNABI **8a** in 61% yield.[87]

Scheme 1. Synthesis of DNABIs 5–8.

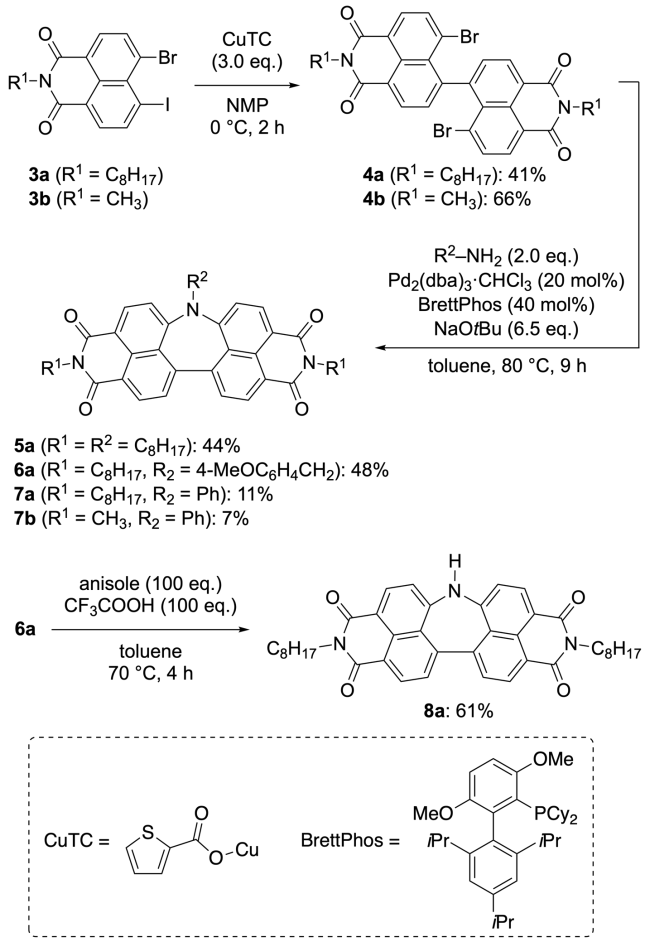

Structural Analysis. The structures of *N*-octyl-substituted DNABI **5a** and *N*-phenyl-substituted DNABI **7b** were unambiguously determined by single-crystal X-ray diffraction analyses (Figure 2). Selected bond lengths and torsion angles are summarized in Table 1. *N*-Octyl-substituted DNABI **5a** adopts a bent structure, in which the central nitrogen atom protrudes from the π-surface, with a dihedral angle of 168° between the two naphthalene units. Importantly, the two naphthalene units are not equivalent, as evident from the different C–N bond lengths *d* (1.431(4) Å) and *d*′ (1.402(3) Å) as well as the dihedral angles φ (36°) and φ′ (23°). Structural optimizations of **5b**, which is a model molecule having methyl groups on the nitrogen atoms instead of octyl groups, by DFT calculations were able to reproduce the nonsymmetric conformation. Consequently, the structural nonsymmetry of **5a** should not arise from crystal-packing forces. On the other hand, *N*-phenyl-substituted DNABI **7b** adopts a twisted nonsymmetric structure in the solid state. However, the DFT optimization of **7b** resulted in a symmetrical conformation, which suggests that **5a** is intrinsically nonsymmetric, while **7b** is symmetric.

To explore the origin of the structural difference between *N*-alkyl-substituted DNABIs **5a,b** and *N*-phenyl-substituted DNABI **7b**, we simulated the structure of *N*-unsubstituted DNABI **8b** (Figure S31). The DFT calculations suggested that the symmetric twisted conformation is energetically more favorable than the nonsymmetric bent structure as in the case of **7b**. This result indicates that the bent structure of **5b** should be ascribed to the substituent effect of the *N*-alkyl

group on the central nitrogen atom. Indeed, replacement of the proton on the central nitrogen atom of **8b** with a methyl group should generate severe intramolecular repulsion between the methyl protons and the adjacent aromatic C–H protons. This situation is due to the symmetrical mismatch between the C_2-symmetric twisted structure and the C_3-symmetric methyl group. A subsequent structural optimization of the *N*-methyl derivative led to a nonsymmetric bent structure. Consequently, we concluded that the structural difference between **5a,b** and **7b** originates from steric repulsion associated with the symmetry around the central nitrogen atom.

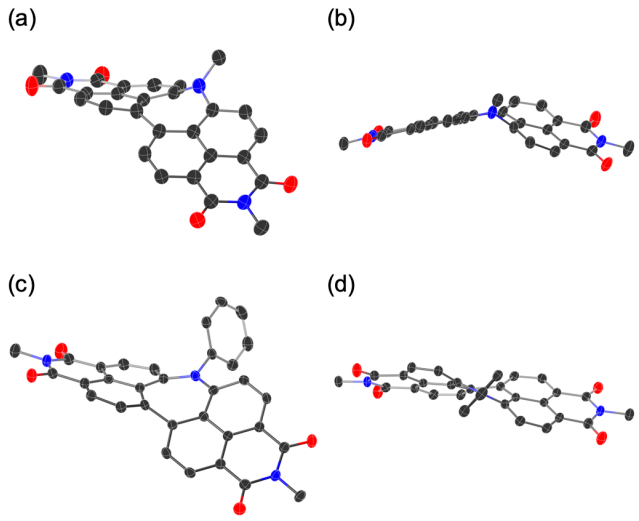

Figure 2. X-ray crystal structures of **5a** and **7b**. (a) Diagonal and (b) side views of **5a**. (c) Diagonal and (d) side views of **7b**. Thermal ellipsoids are shown at 50% probability and all hydrogen atoms and heptyl groups are omitted for clarity.

Table 1. Selected bond lengths and torsion angles in the crystal structures and optimized structures of 5a, 5b, and 7b.

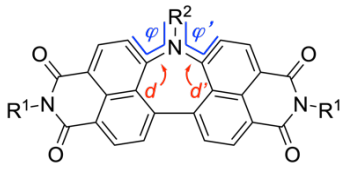

	5a (exp.) and **5b** (calc.)		**7b**	
	exp.[a]	calc.[b]	exp.[a]	calc.[b]
d [Å]	1.431(4)	1.413	1.460(5)	1.407
d' [Å]	1.402(3)	1.397	1.408(3)	1.406
φ [°]	36	33	20	13
φ' [°]	23	20	5	13

[a] X-ray crystal structures. [b] Structures were optimized by DFT calculations at the M06-2X/6-311G(2d,p) level of theory. Octyl groups were replaced by methyl groups in order to simplify the calculations.

Electronic Absorption Spectra. The UV/Vis absorption spectra of **5a**, **7a**, **8a**, and PBI **9** are shown in Figure 3. *N*-Octyl-substituted DNABI **5a**, *N*-phenyl-substituted DNABI **7a**, and *N*-unsubstituted DNABI **8a** exhibit broad absorption bands that tail to ca. 550 nm, which are remarkably red-shifted relative to those of 4-aminonaphthalene monoimides,[88,89] and comparable to that of PBI **9**, i.e., the HOMO–LUMO gaps of **5a**, **7a**, and **8a** are similar to that of **9**. While **7a** and **8a** display two absorption maxima at ca. 410 and 460 nm, **5a** exhibits one absorption maximum at 421 nm together with a weak absorption between 460 and 550 nm. These results suggest that the electronic structures of **7a** and **8a** significantly differ from that of **5a**, which is reminiscent of the structural differences discussed above (*vide supra*).

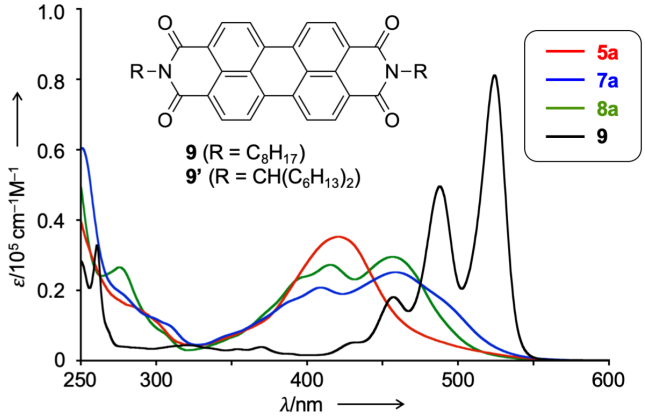

Figure 3. UV/Vis absorption spectra of **5a**, **7a**, **8a**, and **9** in CH_2Cl_2; λ = wavelength; ε = extinction coefficient.

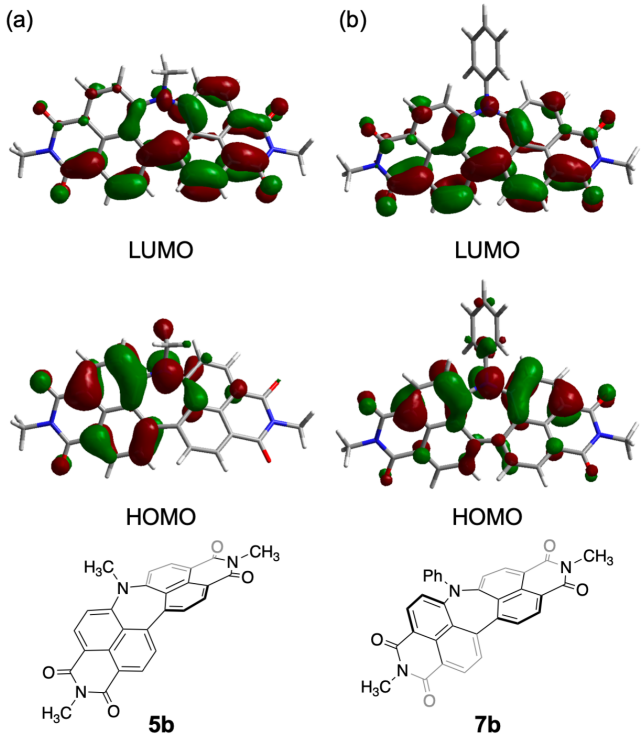

Figure 4. (a) HOMO and LUMO of **5b**. (b) HOMO and LUMO of **7b**; DFT calculations were carried out at the M06-2X/6-311G(2d,p) level of theory.

The calculated frontier orbitals of **5b** and **7b** are shown in Figure 4. The distribution of the frontier orbitals depends on the structural symmetry. While the HOMO and LUMO of **7b** spread over the two naphthalene units, those of **5b** are rather unsymmetrically distributed. The latter feature can most likely be attributed to the anisotropic π-donation of the lone pair on the central nitrogen atom to

one of two naphthalene units. TD-DFT calculations nicely reproduced the experimental spectra (Figure S32), which suggests that the forbidden absorption of **5b** in the long-wavelength region is due to a small orbital overlap between the HOMO and LUMO.

Excited-State Dynamics. The fluorescence quantum yields ($\Phi_{Fl.}$) of **5a** and **7a** in CH_2Cl_2 were determined to be 2.3% and 0.3%, respectively. In toluene, **5a** and **7a** exhibit the $\Phi_{Fl.}$ of 4.3 and 0.5%, respectively. The averaged fluorescence lifetimes of **5a** were measured to be 2.8 and 2.1 ns in toluene and CH_2Cl_2, respectively, by time-correlated single photon counting (TCSPC) technique. The averaged fluorescence lifetimes of **7a** were estimated to be 0.3 and 0.2 ns in toluene and CH_2Cl_2, respectively. In both **5a** and **7a**, the nonradiative decay rate constants were calculated to be twenty to three hundred times larger than radiative decay rate constants (Table S11). These results imply that distorted structures of **5a** and **7a** result in apparently different non-radiative deactivation pathways compared to that of planar PBI, which shows Φ_{Fl} >90% and the fluorescence lifetime of around 5 ns.[68]

To get further insight into the non-emissive features of **5a** and **7a**, we conducted the solvent-dependent transient absorption (TA) measurements in toluene and CH_2Cl_2, respectively (Figures 5 and 6). Upon photoexcitation, both **5a** and **7a** underwent two-step relaxation processes to give a long-lived species, which can be assigned as triplet state. While the initial relaxation processes are independent of the solvent polarity, the subsequent process becomes slower in toluene compared to CH_2Cl_2. Consequently, we assume that the intermediate state is a structurally relaxed charge transfer state (Figure S51).[90,91] Indeed, in a viscous medium (toluene/paraffin oil = 1/9), **5a** and **7a** exhibited the relatively intense fluorescence with the quantum yields of 11 and 2.3%, respectively, which clearly indicates that the conformational change is essential for the triplet state formation. These features should be beneficial to future applications such as viscosity-responsible photofunctional materials.[92,93]

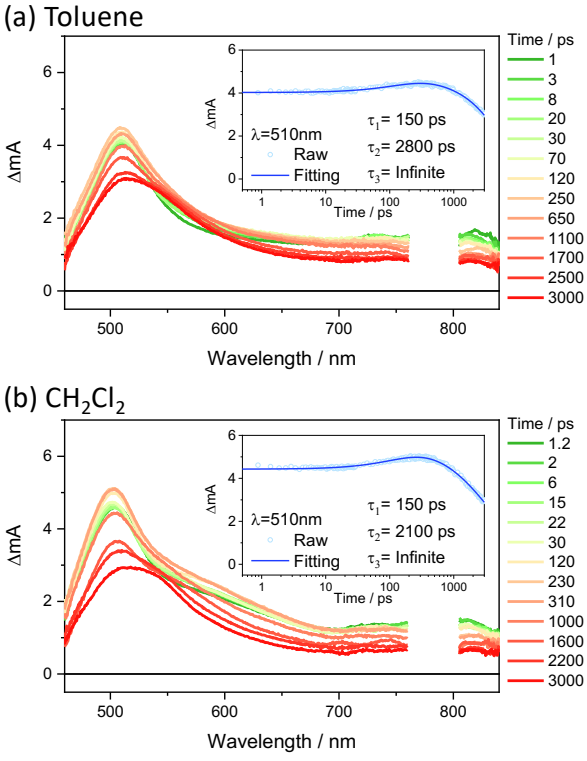

Figure 5. Femtosecond transient absorption (*fs*-TA) spectra of **5a** in (a) toluene and (b) CH_2Cl_2. (λ_{pump} = 400 nm). Inset: decay profiles at 510 nm.

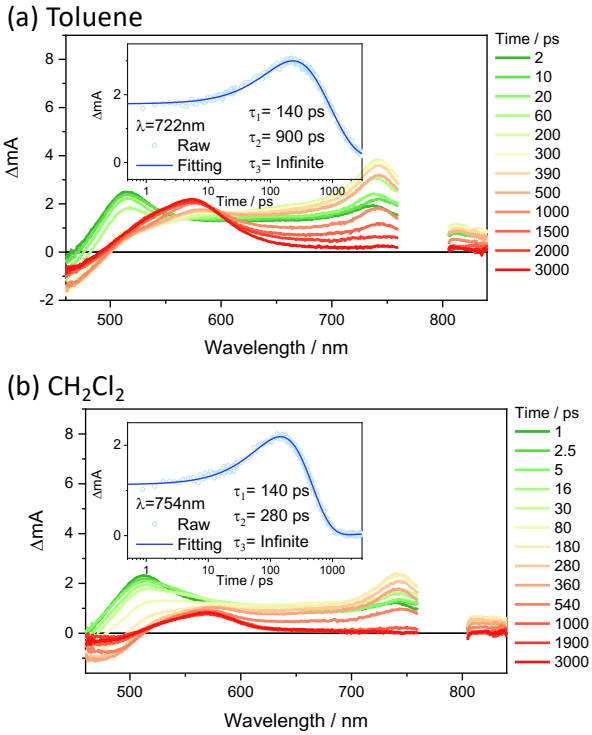

Figure 6. Femtosecond transient absorption (*fs*-TA) spectra of **7a** in (a) toluene and (b) CH_2Cl_2. (λ_{pump} = 400 nm). Inset: decay profiles at 722 and 754 nm in toluene and CH_2Cl_2, respectively.

Table 2. Redox potentials of 5a, 7a, and 9'.[a]

	Oxidation [V]	Reduction [V]		ΔE[b] [eV]
	$E^{1/2}_{ox1}$	$E^{1/2}_{red1}$	$E^{1/2}_{red2}$	
5a	0.99	–1.37	—	2.36
7a	0.85	–1.31	—	2.16
9'	1.24	–1.11	–1.31	2.35

[a] Redox potentials were measured by cyclic voltammetry in anhydrous CH_2Cl_2 using 0.1 M $[Bu_4N][PF_6]$ as the supporting electrolyte and $Ag/AgNO_3$ as the reference electrode. The ferrocene/ferrocenium ion couple was used as an external reference. [b] Electrochemical HOMO–LUMO gap ($\Delta E = E^{1/2}_{ox1} - E^{1/2}_{red1}$).

Electrochemical Properties. The electrochemical properties of **5a**, **7a**, and **9'** were measured by cyclic voltammetry (Figure S29), and selected values are summarized in Table 2. Both *N*-octyl-substituted DNABI **5a** and *N*-phenyl-substituted DNABI **7a** exhibit a set of reversible oxidation and reduction waves. The reduction potentials (**5a**: –1.37 V; **7a**: –1.31 V) are by ca. 0.2 V negatively shifted relative to that of PBI **9'** (–1.11 V), which we attributed to the presence of the electron-rich nitrogen atom. The electrochemical HOMO–LUMO gaps of **5a** (2.36 eV) and **7a** (2.16 eV) are

comparable to that of **9'** (2.35 eV). The calculated HOMO and LUMO energy levels of **5b** and **7b** are higher than those of PBI, which are in accordance with the electrochemical measurements (Figure S30). These results indicate that the electron-rich nitrogen atom acts complementarily to the electron-deficient naphthalene monoimide units, and that both features are compatible, which enables ambipolar redox activity.

Structural Changes in Response to the Application of an Electric Field. Potential structural changes of *N*-methyl-substituted DNABI **5b** and *N*-phenyl-substituted DNABI **7b** were examined by DFT calculations. The global reaction route mapping (GRRM17) program[94] was employed to simulate the intrinsic reaction coordinates. These calculations were conducted at the B3LYP/6-31G(d) level to reduce the calculation costs. The obtained transition state was further optimized by DFT calculations at the M06-2X/6-311G(2d,p). The molecular motion of **5b** encompasses two types of structural changes: (a) inversion of the two inequivalent naphthalene units and (b) flipping of the protruding nitrogen atom (Figure 7). For these structural changes, activation energies of 3.3 and 7.6 kcal mol^{-1} were calculated, respectively. The calculations for *N*-phenyl-substituted DNABI **7b** suggested an inversion of the helical twist with an activation energy of 6.0 kcal mol^{-1} (Figure 8). The ^{1}H NMR spectra of **5a** and **7a** in CD_2Cl_2 at –95 °C revealed a C_2-symmetric pattern with slight broadening (Figures S33 and S34). These results suggest that the molecular motions of **5a** and **7a** are fast on the NMR time scale, even at low temperatures. Activation barriers <10 kcal mol^{-1} were estimated,[95] which is consistent with the theoretical approximation.

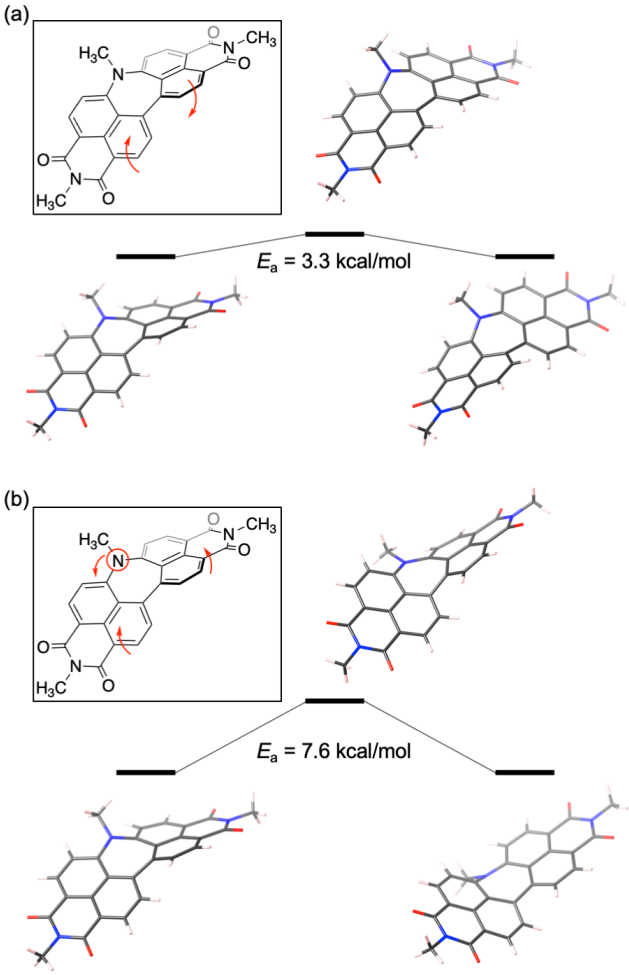

Figure 7. Molecular motion of **5b**: (a) inversion of the two inequivalent naphthalene units and (b) flipping of the protruding nitrogen atom. The absolute energies were calculated at the M06-2X/6-311G(2d,p) level of theory.

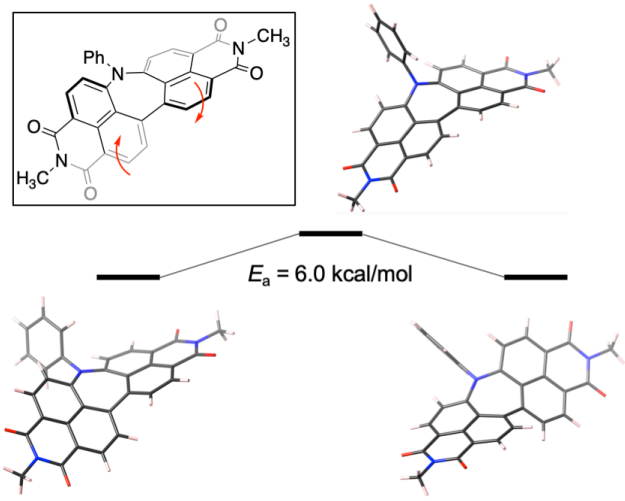

Figure 8. Molecular motion of **7b**. The absolute energies were calculated at the M06-2X/6-311G(2d,p) level of theory.

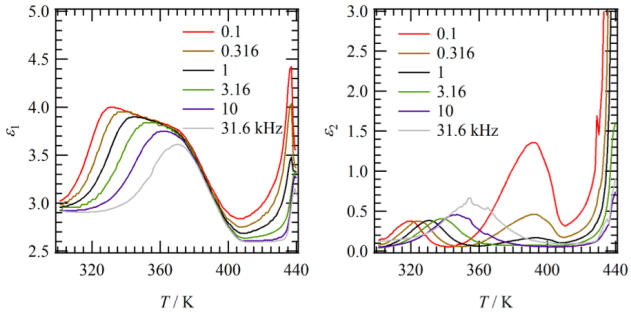

Figure 9. Temperature- and frequency-dependent real (ε_1) and imaginary (ε_2) parts of the dielectric constant for **5a** in the solid state.

The molecular motions of *N*-methyl-substituted DNABI **5b** also change the orientation of its dipole moment. Consequently, we measured the temperature (T)- and frequency (f)-dependent real (ε_1) and imaginary (ε_2) parts of the dielectric constant of **5a** in the solid state in order to examine its response toward the application of an external electric field (Figure 9). In the range of 320–370 K, ε_1 and ε_2 shift to high temperatures with increasing frequency. Differential scanning calorimetry (DSC) and polarized optical microscopy (POM) measurements indicated the presence of a glass phase in this temperature range (Figures 10, S35, and S36). The peak-top temperature (T_{peak}) of ε_1 is proportional to the logarithmic frequency f (Figure S37), which is characteristic for the relaxation of a thermally activated dipole glass.[96] Considering the thermal energy at room temperature ($k_BT \approx 0.6$ kcal/mol), the molecular motion shown in Figure 7a should contribute to the observed dielectric response in the glass. DSC and POM measurements revealed that a further increase of the temperature generated a partial crystal phase in the glass domain at ca. 400 K. The appearance of the ε_2 peak-tops at ca. 390 K should be due to an ordering of the dipole moment associated with the formation of a crystalline phase. On the other hand, *N*-phenyl-substituted DNABI **7a** underwent a phase transition from a solid

phase to an isotropic liquid without passing a glass phase (Figure S38). Furthermore, the temperature-dependent dielectric constants of **7a** did not exhibit a notable response associated with an orientation of the dipole moment (Figure S39).

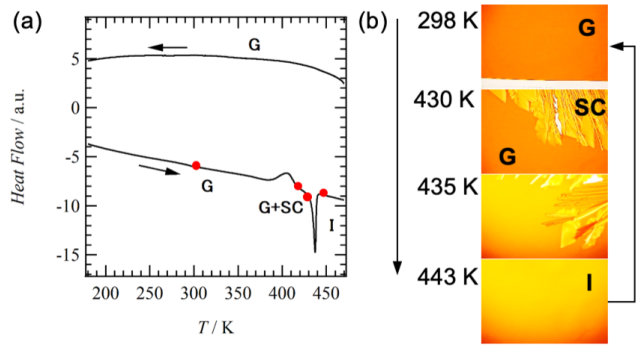

Figure 10. Phase transition behavior of **5a**. (a) DSC chart (third cycle) recorded at a scan rate of 10 K min^{-1}. G, SC, and I refer to glass, crystal, and isotropic liquid, respectively. (b) POM images of G, G+SC, and I under a cross-Nicol optical arrangement.

The conformational dynamics of **5b** disturb the long-range order and crystallization of the closest-packing structure, which forms the dipole glass. Thermal fluctuations of dipole moments occur in the glass state at 320–370 K (first frequency-dependent dielectric relaxation), and a partial crystallization was observed in the glass state at ca. 390 K. The latter phase transition was observed as an exothermic peak at ca. 400 K in the DSC chart, while the coexisting glass and crystal phase was subject to a phase transition to the isotropic liquid at 430 K. On the contrary, **7a**, which exhibits a larger inversion barrier for the structural transformation, stabilized the closest-packing crystalline state in the absence of a dipole glass. The observed molecular dynamics are thus closely correlated to the phase-transition behavior of the dipole glass.

Formation of Hydrogen-Bonding Complexes and Induction of Helical Chirality. The central NH proton of *N*-unsubstituted DNABI **8** should exhibit relatively high acidity owing to the two electron-withdrawing naphthalene monoimide units. To examine the interaction of this proton with a Brønsted base, we conducted titration experiments of **8a** with 1,8-diazabicyclo[5.4.0]undec-7-ene (DBU) in toluene and MeCN/CH_2Cl_2 (v/v = 20/1), respectively (Figure 11). In both cases, the absorption spectra gradually change and isosbestic points are clearly visible. A curve-fitting analysis afforded equilibrium constants (K) of $8.2(2) \times 10^2$ and $3.5(1) \times 10^5$ M^{-1} in toluene and MeCN/CH_2Cl_2, respectively.[97] In toluene, a slightly red-shifted absorption band appeared at 481 nm together with weak tailing up to ca. 700 nm (Figure 11a). Conversely, an intense absorption band was observed at 643 nm in MeCN/CH_2Cl_2 (Figure 11b). Considering the solvent polarity, we assume that the dominant species produced in toluene and MeCN/CH_2Cl_2 are a hydrogen-bonding complex and a deprotonated anion, respectively.[98,99] In contrast, titration in CH_2Cl_2 afforded an ill-defined absorption change that lacked isosbestic points, implying the co-existence of these two species (Figure S40).[100]

To control the helical chirality of the hydrogen-bonding complex, we added the optically active Brønsted base **10**[101–103] to a toluene solution of *N*-unsubstituted DNABI **8a** and monitored the reaction by CD spectroscopy (Figure 12). Interestingly, clear CD signals emerged in the range of 300–650 nm, which indicates that the helicity of the twisted DNABI core was enantiomerically controlled by **10**.[104–108] On the other hand, a DMSO solution of **8a** with **10** as well as a toluene solution of *N*-phenyl-substituted DNABI **7a** with **10** exhibited no identical CD signal (Figures S43 and S44). These results suggest that the formation of a hydrogen-bonding complex involving the central NH unit of **8a** is essential to induce CD signals. The structure of the complex was simulated by DFT calculations, in which the DNABI core was sandwiched by the phenyl and isopropyl groups of the chiral Brønsted base **10** (Figure 13). These DFT calculations suggest that (*M*)-**8a·10** is energetically more favorable than (*P*)-**8a·10**. The simulated CD spectrum of (*M*)-**8a·10** is consistent with the experimental results, i.e., the Cotton effects around 400 and 500 nm, respectively (Figure S47).

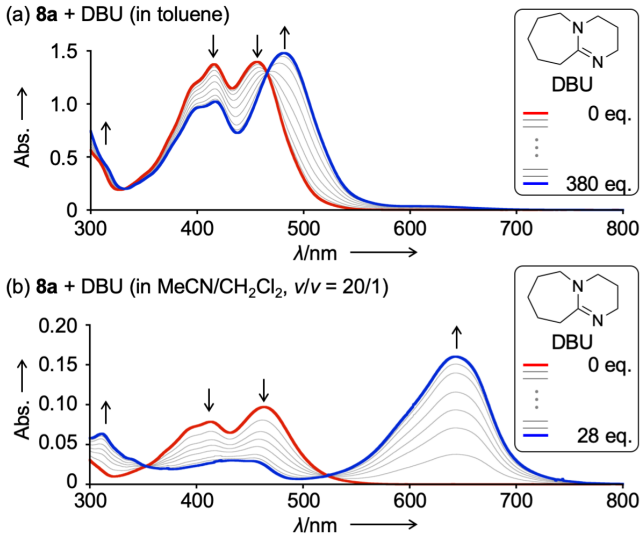

Figure 11. UV/Vis absorption spectral changes during titration of **8a** with DBU at 20 °C in (a) toluene ([**8a**]$_0$ = 5.6×10^{-5} M) and (b) MeCN/CH_2Cl_2 ([**8a**]$_0$ = 3.4×10^{-6} M).

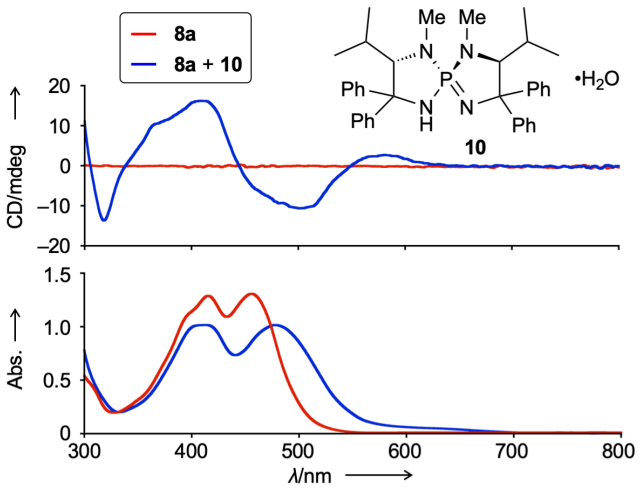

Figure 12. Circular dichroism (CD) (top) and UV/Vis absorption (bottom) spectra of **8a** with **10** in toluene at 25 °C ([**8a**]$_0$ = 5.6×10^{-5} M, [**10**]$_0$ = 2.8×10^{-3} M, d = 1.0 cm).

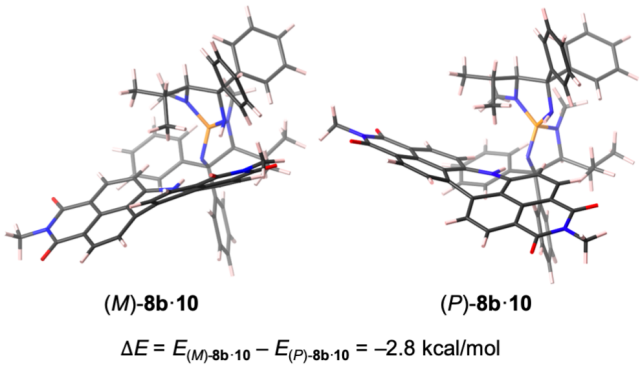

Figure 13. Optimized structures of (*M*)-**8a·10** and (*P*)-**8a·10**; DFT calculations were conducted at the M06-2X/6-311G(2d,p) level of theory. The solvation effect was simulated using the IEFPCM method and toluene as the solvent.

CONCLUSIONS

We synthesized dinaphtho[1,8-bc:1',8'-ef]azepine bisimides (DNABIs) as non-planar perylene bisimide analogues from 4-bromo-5-iodonaphthalene monoimides through copper-mediated homocoupling and a subsequent Buchwald–Hartwig amination as key steps. A detailed structural analysis revealed that depending on the steric effect around the central nitrogen atom, DNABIs adopt one of two conformations. While *N*-unsubstituted DNABI **8** and *N*-phenyl-substituted DNABI **7** adopt a symmetric twisted conformation, *N*-alkyl-substituted DNABI **5** exhibit a nonsymmetric bent conformation. DFT calculations predicted that the former conformation is intrinsically favorable, and that the driving force to provide the latter conformation is most likely due to intramolecular steric repulsion associated with a symmetry mismatch between the C_2-symmetric twisted structure and the C_3-symmetric alkyl groups. UV/Vis spectra and the results of theoretical calculations suggest that the structural differences manifest in different electronic properties. Notably, nonsymmetric DNABI **5a** undergoes unique structural changes in response to the application of an external electric field as its molecular motion is associated with an orientational change of its dipole moment. Moreover, the chiral Brønsted base **10** forms a hydrogen-bonding complex with *N*-unsubstituted DNABI **8a**, which allows controlling the helicity of the twisted core. Further investigations into the incorporation of other heteroatoms into the dinaphtho[1,8-bc:1',8'-ef]heteropine bisimide core are currently in progress in our laboratory and the results will be reported in due course.

ASSOCIATED CONTENT

Supporting Information

The Supporting Information is available free of charge on the ACS Publications website.
Experimental details and spectral data for all new compounds (PDF).
Crystallographic data for **5a** (CIF).
Crystallographic data for **7b** (CIF)

AUTHOR INFORMATION

Corresponding Author

akutagawa@tohoku.ac.jp, dongho@yonsei.ac.kr, fukui@chembio.nagoya-u.ac.jp, hshino@chembio.nagoya-u.ac.jp

Notes

The authors declare no competing financial interest.

ACKNOWLEDGMENT

This work was supported by JSPS KAKENHI grant JP17H01190 (H.S.) and JP19H00886 (T.A.). T.A. acknowledges JST CREST Grant Number JPMJCR18I4 and "Dynamic Alliance for Open Innovation Bridging Human, Environment and Materials" from MEXT. N.F. gratefully acknowledges the Tatematsu Foundation for financial support. The authors acknowledge Prof. Dr. Makoto Yamashita and Dr. Katsunori Suzuki for XRD measurements, as well as Prof. Dr. Eiji Yashima and Dr. Daisuke Taura for CD measurements. We also thank Mr. Fumito Ueoka in Ooi group for preparation of **10**. The work at Yonsei University was supported by the Strategic Research (NRF2016R1E1A1A01943379) through the National Research Foundation of Korea (NRF) funded by the Ministry of Science.

REFERENCES

(1) Gingras, M. One Hundred Years of Helicene Chemistry. Part 3: Applications and Properties of Carbohelicenes. *Chem. Soc. Rev.* **2013**, *42*, 1051–1095.
(2) Scott, L. T. Methods for the Chemical Synthesis of Fullerenes. *Angew. Chem., Int. Ed.* **2004**, *43*, 4994–5007.
(3) Kawase, T.; Kurata, H. Ball-, Bowl-, and Belt-Shaped Conjugated Systems and Their Complexing Abilities: Exploration of the Concave–Convex π-π Interaction. *Chem. Rev.* **2006**, *106*, 5250–5273.
(4) Wu, Y.-T.; Siegel, J. S. Aromatic Molecular-Bowl Hydrocarbons: Synthetic Derivatives, Their Structures, and Physical Properties. *Chem. Rev.* **2006**, *106*, 4843–4867.
(5) Pascal, R. A. Twisted Acenes. *Chem. Rev.* **2006**, *106*, 4809–4819.
(6) Shen, Y.; Chen, C.-F. Helicenes: Synthesis and Applications. *Chem. Rev.* **2012**, *112*, 1463–1535.
(7) Bodwell, G. J. Extraordinary Transformations to Achieve the Synthesis of Remarkable Aromatic Compounds. *Chem. Rec.* **2014**, *14*, 547–567.
(8) Miao, Q. Heptagons in Aromatics: From Monocyclic to Polycyclic. *Chem. Rec.* **2015**, *15*, 1156–1159.
(9) Segawa, Y.; Yagi, A.; Matsui, K.; Itami, K. Design and Synthesis of Carbon Nanotube Segments. *Angew. Chem., Int. Ed.* **2016**, *55*, 5136–5158.
(10) Hiroto, S. Innovative Synthesis and Functions of Curved π-Conjugated Molecules. *Bull. Chem. Soc. Jpn.* **2018**, *91*, 829–838.
(11) Saito, M.; Shinokubo, H.; Sakurai, H. Figuration of Bowl-shaped π-Conjugated Molecules: Properties and Functions. *Mater. Chem. Front.* **2018**, *2*, 635–661.
(12) Márquez, I. R.; Castro-Fernández, S.; Millán, A.; Campaña, A. G. Synthesis of Distorted Nanographenes Containing Seven- and Eight-membered Carbocycles. *Chem. Commun.* **2018**, *54*, 6705–6718.
(13) Majewski, M. A.; Stępień, M. Bowls, Hoops, and Saddles: Synthetic Approaches to Curved Aromatic Molecules. *Angew. Chem., Int. Ed.* **2019**, *58*, 86–116.
(14) Barth, W. E.; Lawton, R. G. Dibenzo[*ghi*,*mno*]fluoranthene. *J. Am. Chem. Soc.* **1966**, *88*, 380–381.
(15) Fernández-García, J. M.; Evans, P. J.; Filippone, S.; Herranz, M. Á.; Martín, N. Chiral Molecular Carbon Nanostructures. *Acc. Chem. Res.* **2019**, *52*, 1565–1574.
(16) Sakurai, H.; Daiko, T.; Hirao, T. A Synthesis of Sumanene, a Fullerene Fragment. *Science* **2003**, *301*, 1878.
(17) Jasti, R.; Bhattacharjee, J.; Neaton, J. B.; Bertozzi, C. R. Synthesis, Characterization, and Theory of [9]-, [12]-, and [18]Cycloparaphenylene: Carbon Nanohoop Structures. *J. Am. Chem. Soc.* **2008**, *130*, 17646–17647.
(18) Takaba, H.; Omachi, H.; Yamamoto, Y.; Bouffard, J.; Itami, K. Selective Synthesis of [12]Cycloparaphenylene. *Angew. Chem., Int. Ed.* **2009**, *48*, 6112–6116.
(19) Scott, L. T.; Jackson, E. A.; Zhang, Q.; Steinberg, B. D.; Bancu, M.; Li, B. A Short, Rigid, Structurally Pure Carbon Nanotube by Stepwise Chemical Synthesis. *J. Am. Chem. Soc.* **2012**, *134*, 107–110.
(20) Povie, G.; Segawa, Y.; Nishihara, T.; Miyauchi, Y.; Itami, K. Synthesis of a Carbon Nanobelt. *Science* **2017**, *356*, 172–175.
(21) Lu, J.; Ho, D. M.; Vogelaar, N. J.; Kraml, C. M.; Pascal, R. A. A Pentacene with a 144° Twist. *J. Am. Chem. Soc.* **2004**, *126*, 11168–11169.

(22) Torricelli, F.; Bosson, J.; Besnard, C.; Chekini, M.; Bürgi, T.; Lacour, J. Modular Synthesis, Orthogonal Post-Functionalization, Absorption, and Chiroptical Properties of Cationic [6]Helicenes. *Angew. Chem., Int. Ed.* **2013**, *52*, 1796–1800.

(23) Unikela, K. S.; Roemmele, T. L.; Houska, V.; McGrath, K. E.; Tobin, D. M.; Dawe, L. N.; Boeré, R. T.; Bodwell, G. J. Gram-Scale Synthesis and Highly Regioselective Bromination of 1,1,9,9-Tetramethyl[9](2,11)teropyrenophane. *Angew. Chem., Int. Ed.* **2018**, *57*, 1707–1711.

(24) Bedi, A.; Shimon, L. J. W.; Gidron, O. Helically Locked Tethered Twistacenes. *J. Am. Chem. Soc.* **2018**, *140*, 8086–8090.

(25) Nakakuki, Y.; Hirose, T.; Matsuda, K. Synthesis of a Helical Analogue of Kekulene: A Flexible π-Expanded Helicene with Large Helical Diameter Acting as a Soft Molecular Spring. *J. Am. Chem. Soc.* **2018**, *140*, 15461–15469.

(26) Yuan, C.; Saito, S.; Camacho, C.; Irle, S.; Hisaki, I.; Yamaguchi, S. A π-Conjugated System with Flexibility and Rigidity That Shows Environment-Dependent RGB Luminescence. *J. Am. Chem. Soc.* **2013**, *135*, 8842–8845.

(27) Feng, C.-N.; Kuo, M.-Y.; Wu, Y.-T. Synthesis, Structural Analysis, and Properties of [8]Circulenes. *Angew. Chem., Int. Ed.* **2013**, *52*, 7791–7794.

(28) Sakamoto, Y.; Suzuki, T. Tetrabenzo[8]circulene: Aromatic Saddles from Negatively Curved Graphene. *J. Am. Chem. Soc.* **2013**, *135*, 14074–14077.

(29) Evans, P. J.; Ouyang, J.; Favereau, L.; Crassous, J.; Fernández, I.; Perles, J.; Marín, N. Synthesis of a Helical Bilayer Nanographene. *Angew. Chem. Int. Ed.* **2018**, *57*, 6774–6779.

(30) Gallego, M.; Calbo, J.; Aragó, J.; Calderon, R. M. K.; FLiquido, F. H.; Iwamoto, T.; Greene, A. K.; Jackson, E. A.; Pérez, E. M.; Ortí, E.; Guldi, D. M.; Scott, L. T.; Martín, N. Electron Transfer in a Supramolecular Associate of a Fullerene Fragment. *Angew. Chem. Int. Ed.* **2014**, *53*, 2170–2175.

(31) Schmidt, B. M.; Seki, S.; Topolinski, B.; Ohkubo, K.; Fukuzumi, S.; Sakurai, H.; Lentz, D. Electronic Properties of Trifluoromethylated Corannulenes. *Angew. Chem., Int. Ed.* **2012**, *51*, 11385–11388.

(32) Amaya, T.; Seki, S.; Moriuchi, T.; Nakamoto, K.; Nakata, T.; Sakane, H.; Saeki, A.; Tagawa, S.; Hirao, T. Anisotropic Electron Transport Properties in Sumanene Crystal. *J. Am. Chem. Soc.* **2009**, *131*, 408–409.

(33) Wakamiya, A.; Nishimura, H.; Fukushima, T.; Suzuki, F.; Saeki, A.; Seki, S.; Osaka, I.; Sasamori, T.; Murata, M.; Murata, Y.; Kaji, H. On-Top π-Stacking of Quasiplanar Molecules in Hole-Transporting Materials: Inducing Anisotropic Carrier Mobility in Amorphous Films. *Angew. Chem., Int. Ed.* **2014**, *23*, 5800–5804.

(34) Nishimura, H.; Hasegawa, Y.; Wakamiya, A.; Murata, Y. Development of Transparent Organic Hole-transporting Materials Using Partially Oxygen-bridged Triphenylamine Skeletons. *Chem. Lett.* **2017**, *46*, 817–820.

(35) Mizyed, S.; Georghiou, P. E.; Bancu, M.; Cuadra, B.; Rai, A. K.; Cheng, P.; Scott, L. T. Embracing C_{60} with Multiarmed Geodesic Partners. *J. Am. Chem. Soc.* **2001**, *123*, 12770–12774.

(36) Sygula, A.; Fronczek, F. R.; Sygula, R.; Rabideau, P. W.; Olmstead, M. M. A Double Concave Hydrocarbon Buckycatcher. *J. Am. Chem. Soc.* **2007**, *129*, 3842–3843.

(37) Yamamura, M.; Saito, T.; Nabeshima, T. Phosphorus-Containing Chiral Molecule for Fullerene Recognition Based on Concave/Convex Interaction. *J. Am. Chem. Soc.* **2014**, *136*, 14299–14306.

(38) Takeda, M.; Hiroto, S.; Yokoi, H.; Lee, S.; Kim, D.; Shinokubo, H. Azabuckybowl-Based Molecular Tweezers as C_{60} and C_{70} Receptors. *J. Am. Chem. Soc.* **2018**, *140*, 6336–6342.

(39) Miyajima, D.; Tashiro, K.; Araoka, F.; Takezoe, H.; Kim, J.; Kato, K.; Takata, M.; Aida, T. Liquid Crystalline Corannulene Responsive to Electric Field. *J. Am. Chem. Soc.* **2009**, *131*, 44–45.

(40) Kang, J.; Miyajima, D.; Mori, T.; Inoue, Y.; Itoh, Y.; Aida, T. A Rational Strategy for the Realization of Chain-growth Supramolecular Polymerization. *Science* **2015**, *347*, 646–651.

(41) Yamamoto, K.; Harada, T.; Nakazaki, M.; Naka, T.; Kai, Y.; Harada, S.; Kasai, N. Synthesis and Characterization of [7]Circulene. *J. Am. Chem. Soc.* **1983**, *105*, 7171–7172.

(42) Yamamoto, K.; Harada, T.; Okamoto, Y.; Chikamatsu, H.; Nakazaki, M.; Kai, Y.; Nakao, T.; Tanaka, M.; Harada, S.; Kasai, N. Synthesis and Molecular Structure of [7]Circulene. *J. Am. Chem. Soc.* **1988**, *110*, 3578–3584.

(43) Yamamoto, K.; Saitho, Y.; Iwaki, D.; Ooka, T. [7.7]Circulene, a Molecule Shaped Like a Figure of Eight. *Angew. Chem., Int. Ed. Engl.* **1991**, *30*, 1173–1174.

(44) Yamamoto, K. Extended Systems of Closed Helicene. Synthesis and Characterization of [7] and [7.7]-Circulene. *Pure Appl. Chem.* **1993**, *65*, 157–163.

(45) Mughal, E. U.; Kuck, D. Merging Tribenzotriquinacene with Hexa-*peri*-hexabenzocoronene: a Cycloheptatriene Unit Generated by Scholl Reaction. *Chem. Commun.* **2012**, *48*, 8880–8882.

(46) Luo, J.; Xu, X.; Mao, R.; Miao, Q. Curved Polycyclic Aromatic Molecules That Are π-Isoelectronic to Hexabenzocoronene. *J. Am. Chem. Soc.* **2012**, *134*, 13796–13803.

(47) Pradhan, A.; Dechambenoit, P.; Bock, H.; Durola, F. Twisted Polycyclic Arenes by Intramolecular Scholl Reactions of C3-Symmetric Precursors. *J. Org. Chem.* **2013**, *78*, 2266–2274.

(48) Cheung, K. Y.; Xu, X.; Miao, Q. Aromatic Saddles Containing Two Heptagons. *J. Am. Chem. Soc.* **2015**, *137*, 3910–3914.

(49) Kawasumi, K.; Zhang, Q.; Segawa, Y.; Scott, L. T.; Itami, K. A Grossly Warped Nanographene and the Consequences of Multiple Odd-membered-ring Defects. *Nat. Chem.* **2013**, *5*, 739–744.

(50) Kato, K.; Segawa, Y.; Scott, L. T.; Itami, K. Synthesis, Properties, and Packing Structures of Corannulene-Based π-Systems Containing Heptagons. *Chem.-Asian J.* **2015**, *10*, 1635–1639.

(51) Żyła, M.; Gońka,E.; Chmielewski, P. J.; Cybińska, J.; Stępień, M. Synthesis of a Peripherally Conjugated 5-6-7 Nanographene. *Chem. Sci.* **2016**, *7*, 286–294.

(52) Gu, X.; Li, H.; Shan, B.; Liu, Z.; Miao, Q. Synthesis, Structure, and Properties of Tetrabenzo[7]circulene. *Org. Lett.* **2017**, *19*, 2246–2249.

(53) Ip, H.-W.; Ng, C.-F.; Chow, H.-F.; Kuck, D. Three-Fold Scholl-Type Cycloheptatriene Ring Formation around a Tribenzotriquinacene Core: Toward Warped Graphenes. *J. Am. Chem. Soc.* **2016**, *138*, 13778–13781.

(54) Márquez, R.; Fuentes, N.; Cruz, C. M.; Puente-Muñoz, V.; Satorrios, L.; Marcos, M. L.; Choquesillo-Lazarte, D.; Biel, B.; Crovetto, L.; Gómez-Bengoa, E.; González, M. T.; Martin, R.; Cuerva, J. M.; Campaña, A. G. Versatile Synthesis and Enlargement of Functionalized Distorted Haptagon-containing Nanographenes. *Chem. Sci.* **2017**, *8*, 1068–1074.

(55) Cruz, C. M.; Castro-Fernández, S.; Maçôas, E.; Cuerva, J. M.; Campaña, A. G. Undecabenzo[7]superhelicene: A Helical Nanographene Ribbon as a Circularly Polarized Luminescence Emitter. *Angew. Chem., Int. Ed.* **2018**, *57*, 14782–14786.

(56) Pun, S. H.; Chan, C. K.; Luo, J.; Liu, Z.; Miao, Q. A Dipleiadiene-Embedded Aromatic Saddle Consisting of 86 Carbon Atoms. *Angew. Chem., Int. Ed.* **2018**, *57*, 1581–1586.

(57) Cruz, C. M.; Márquez, I. R.; Castro-Fernández, S.; Cuerva, J. M.; Maçôas, E.; Campaña, A. G. A Triskelion-Shaped Saddle-Helix Hybrid Nanographene. *Angew. Chem., Int. Ed.* **2019**, *58*, 8068–8072.

(58) Fukui, N.; Kim, T.; Kim, D.; Osuka, A. Porphyrin Arch-Tapes: Synthesis, Contorted Structures, and Full Conjugation. *J. Am. Chem. Soc.* **2017**, *139*, 9075–9088.

(59) Fukui, N.; Osuka, A. Singly and Doubly 1,2-Phenylene-Inserted Porphyrin Arch-Tape Dimers: Synthesis and Highly Contorted Structures. *Angew. Chem., Int. Ed.* **2018**, *57*, 6304–6308.

(60) Fukui, N.; Osuka, A. Singly and Doubly Sulfone-Inserted Porphyrin Arch-Tape Dimers. *Bull. Chem. Soc. Jpn.* **2018**, *91*, 1131–1137.

(61) Stępień, M.; Gońka, E.; Żyła, M.; Sprutta, N. Heterocyclic Nanographenes and Other Polycyclic Heteroaromatic Compounds: Synthetic Routes, Properties, and Applications. *Chem. Rev.* **2017**, *117*, 3479–3716.

(62) Hirai, M.; Tanaka, N.; Sakai, M.; Yamaguchi, S. Structurally Constrained Boron-, Nitrogen-, Silicon-, and Phosphorus-Centered Polycyclic π-Conjugated Systems. *Chem. Rev.* **2019**, *119*, 8291–8331.

(63) Würthner, F. Perylene Bisimide Dyes as Versatile Building Blocks for Functional Supramolecular Architectures. *Chem. Commun.* **2004**, 1564–1579.

(64) Weil, T.; Vosch, T.; Hofkens, J.; Peneva, K.; Müllen, K. The Rylene Colorant Family—Tailored Nanoemitters for Photonics Research and Applications. *Angew. Chem., Int. Ed.* **2010**, *49*, 9068–9093.

(65) Zhan, X.; Facchetti, A.; Barlow, S.; Marks, T. J.; Ratner, M. A.; Wasielewski, M. R.; Marder, S. R. Rylene and Related Diimides for Organic Electronics. *Adv. Mater.* **2011**, *23*, 268–284.

(66) Würthner, F.; Stolte, M. Naphthalene and Perylene Diimides for Organic Transistors. *Chem. Commun.* **2011**, *47*, 5109–5115.

(67) Liu, Z.; Zhang, G.; Cai, Z.; Chen, X.; Luo, H.; Li, Y.; Wang, J.; Zhang, D. New Organic Semiconductors with Imide/Amide-Containing Molecular Systems. *Adv. Mater.* **2014**, *26*, 6965–6977.

(68) Würthner, F.; Saha-Möller, C.; Fimmel, B.; Ogi, S.; Leowanawat, P.; Schmidt, D. Perylene Bisimide Dye Assemblies as Archetype Functional Supramolecular Materials. *Chem. Rev.* **2016**, *116*, 962–1052.

(69) Würthner, F. Bay-substituted Perylene Bisimides: Twisted Fluorophores for Supramolecular Chemistry. *Pure Appl. Chem.* **2006**, *78*, 2341–2349.

(70) Huang, C.; Barlow, S.; Marder, S. R. Perylene-3,4,9,10-tetracarboxylic Acid Diimides: Synthesis, Physical Properties, and Use in Organic Electronics. *J. Org. Chem.* **2011**, *76*, 2386–2407.

(71) Qian, H.; Wang, Z.; Yue, W.; Zhu, D. Exceptional Coupling of Tetrachloroperylene Bisimide: Combination of Ullmann Reaction and C–H Transformation. *J. Am. Chem. Soc.* **2007**, *129*, 10664–10665.

(72) Jones, B. A.; Facchetti, A.; Wasielewski, M. R.; Marks, T. J. Tuning Orbital Energetics in Arylene Diimide Semiconductors. Materials Design for Ambient Stability of n-Type Charge Transport. *J. Am. Chem. Soc.* **2007**, *129*, 15259–15278.

(73) Qian, H.; Negri, F.; Wang, C.; Wang, Z. Fully Conjugated Tri(Perylene Bisimides): An Approach to the Construction of *n*-Type Graphene Nanoribbons. *J. Am. Chem. Soc.* **2008**, *130*, 17970–17976.

(74) Zhen, Y.; Yue, W.; Li, Y.; Jiang, W.; Motta, S. D.; Donato, E. D.; Negri, F.; Wang, Z. Chiral Nanoribbons based on Doubly-linked Oligoperylene Bisimides. *Chem. Commun.* **2010**, *46*, 6078–6080.

(75) Zhong, Y.; Kumar, B.; Oh, S.; Trinh, M. T.; Wu, Y.; Elbert, K.; Li, P.; Zhu, X.; Xiao, S.; Ng, F.; Steigerwald, M. L.; Nuckolls, C. Helical Ribbons for Molecular Electronics. *J. Am. Chem. Soc.* **2014**, *136*, 8122–8130.

(76) Jiang, W.; Ye, L.; Li, X.; Xiao, C.; Tan, F.; Zhao, W.; Hou, J.; Wang, Z. Bay-linked Perylene Bisimides as Promising Non-fullerene Acceptors for Organic Solar Cells. *Chem. Commun.* **2014**, *50*, 1024–1026.

(77) Cai, Y.; Huo, L.; Sun, X.; Wei, D.; Tang, M.; Sun, Y. High Performance Organic Solar Cells Based on a Twisted Bay-Substituted Tetraphenyl Functionalized Perylenediimide Electron Acceptor. *Adv. Energy. Mater.* **2015**, *5*, 1500032.

(78) Zhong, Y.; Trinh, M. T.; Chen, R.; Purdum, G. E.; Khlyabich, P. P.; Sezen, M.; Oh, S.; Zhu, H.; Fowler, B.; Zhang, B.; Wang, W.; Nam, C.-Y.; Sfeir, M. Y.; Black, C. T.; Steigerwald, M. L.; Loo, Y.-L.; Ng, F.; Zhu, X.-Y.; Nuckolls, C. Molecular Helices as Electron Acceptors in High-performance Bulk Heterojunction Solar Cells. *Nat. Commun.* **2015**, *6*, 8242.

(79) Schuster, N. J.; Paley, D. W.; Jockusch, S.; Ng, F.; Steigerwald, M. L.; Nuckolls, C. Electron Delocalization in Perylene Diimide Helicenes. *Angew. Chem., Int. Ed.* **2016**, *55*, 13519–13523.

(80) Dobelmann, L.; Parham, A. H.; Büsing, A.; Buchholz, H.; König, B. First Synthesis of Naphthalene Annulated Oxepins. *RSC Adv.* **2014**, *4*, 60473–60477.

(81) Schickedanz, K.; Radtke, J.; Bolte, M.; Lerner, H.-W.; Wagner, M. Facile Route to Quadruply Annulated Borepins. *J. Am. Chem. Soc.* **2017**, *139*, 2842–2851.

(82) Duan, L.; Xu, Y.; Qian, X.; Zhang, Y.; Liu, Y. Novel Naphthalimide Derivatives with Near-infrared Emission: Synthesis via Photochemical Cycloaromatization, Fluorescence in Solvents and Living Cell. *Tetrahedron Lett.* **2009**, *50*, 22–25.

(83) Liu, L.; Zhang, C.; Zhao, J. The Effect of the Regioisomeric Naphthalimide Acetylide Ligands on the Photophysical Properties of N^N Pt(II) Bisacetylide Complexes. *Dalton Trans.* **2014**, *43*, 13434–13444.

(84) Nelson, T. D.; Crouch, R. D. Cu, Ni, and Pd-mediated Homocoupling Reactions in Biaryl Syntheses: The Ullmann Reaction. *Org. React.* **2004**, *63*, 265–555.

(85) Surry, D. S.; Buchwald, S. L. Dialkylbiaryl Phosphines in Pd-catalyzed Amination: A User's Guide. *Chem. Sci.* **2011**, *2*, 27–50.

(86) Hartwig, J. F. Evolution of a Fourth Generation Catalyst for the Amination and Thioetherification of Aryl Halides. *Acc. Chem. Res.* **2008**, *41*, 1534–1544.

(87) De Medeiros, E. F.; Herbert, J. M.; Taylor, R. J. K. The Synthesis and Absolute Configuration of the Novel Ichthyotoxic Diacylglycerols, Umbraculumin A and Umbraculumin C. *J. Chem. Soc. Perkin Trans. 1* **1991**, 2725–2730.

(88) Alexiou, M.; Tyman, J.; Wilson, I. Nucleophilic Displacement of the Nitro Group in 2- and 4-Nitronaphtalic-1,8-anhydrides and Derivatives. *Tetrahedron Lett.* **1981**, *22*, 2303–2306.

(89) Greenfield, S. R.; Svec, W. A.; Gosztola, D.; Wasielewski, M. R. Multistep Photochemical Charge Separation in Rod-like Molecules Based on Aromatic Imides and Diimides. *J. Am. Chem. Soc.* **1996**, *118*, 6767–6777.

(90) Dimitrov, S. D.; Wheeler, S.; Niedzialek, D.; Schroeder, B. C.; Utzat, H.; Frost, J. M.; Yao, J.; Gillett, A.; Tuladhar, P.; McCulloch, I.; Nelson, J.; Durrant, J. R. Polaron Pair Mediated Triplet Generation in Polymer/Fullerene Blends. *Nat. Commun.* **2015**, *6*, 6501.

(91) Zhang, Y.; Oh, J.; Wang, K.; Shin, D.; Zhan, X.; Zheng, Y.; Kim, D.; Jiang, J. The First Porphyrin–Subphthalocyaninatoboron(III)-fused Hybrid with Unique Conformation and Intramolecular Charge Transfer Behavior. *Chem. Commun.* **2016**, *52*, 10517.

(92) Kuimova, M. K. Mapping Viscosity in Cells Using Molecular Rotors. *Phys. Chem. Chem. Phys.* **2012**, *14*, 12671–12686.

(93) Yang, Z.; Cao, J.; He, Y.; Yang, J. H.; Kim, T.; Peng, X.; Kim, J. S. Macro-/micro-environment-sensitive Chemosensing and Biological Imaging. *Chem. Soc. Rev.* **2014**, *43*, 4563.

(94) Maeda, S.; Harabuchi, Y.; Takagi, M.; Saita, K.; Suzuki, K.; Ichino, T.; Sumiya, Y.; Sugiyama, K.; Ono, Y. Implementation and Performance of the Artificial Force Induced Reaction Method in the GRRM17 Program. *J. Comp. Chem.* **2018**, *39*, 233–250.

(95) Gasparro, F. P.; Kolodny, N. H. NMR Determination of the Rotational Barrier in *N*,*N*-dimethylacetamide. *J. Chem. Educ.* **1977**, *54*, 258–261.

(96) Kleemann, W.; Kütz, S.; Rytz, D. Cluster Glass and Domain State Properties of $KTaO_3$ Li. *Europhys. Lett.*, **1987**, *4*, 239.

(97) Thordarson, P. Determining Association Constants from Titration Experiments in Supramolecular Chemistry. *Chem. Soc. Rev.* **2011**, *40*, 1305–1323.

(98) Ratajczak, H.; Sobczyk, L. Dipole Moments of Hydrogen-Bonded Complexes and Proton-Transfer Effect. *J. Chem. Phys.* **1969**, *59*, 556–557.

(99) Zundel, G.; Fritsch, J. Environmental Interaction of Hydrogen Bonds Showing a Large Proton Polarizability. Molecular Processes and the Thermodynamics of Acid Dissociation. *J. Phys. Chem.* **1984**, *88*, 6295–6302.

(100) This assumption is supported by the results of the CD measurements; for details, see Figure S45.

(101) Uraguchi, D.; Sakaki, S.; Ooi, T. Chiral Tetraaminophosphonium Salt-mediated Asymmetric Direct Henry Reaction. *J. Am. Chem. Soc.* **2007**, *129*, 12392–12393.

(102) Uraguchi, D.; Ueki, Y.; Ooi, T. Chiral Tetraaminophosphonium Carboxylate-catalyzed Direct Mannich-type Reaction. *J. Am. Chem. Soc.* **2008**, *130*, 14088–14089.

(103) Uraguchi, D.; Ueki, Y.; Ooi, T. Chiral Organic Ion Pair Catalysts Assembled Through a Hydrogen-Bonding Network. *Science* **2009**, *326*, 120–123.

(104) Hembury, G. A.; Borovkov, V. V.; Inoue, Y. Chirality-sensing Supramolecular Systems. *Chem. Rev.* **2008**, *108*, 1–73.

(105) Yashima, E.; Ousaka, N.; Taura, D.; Shimomura, K.; Ikai, T.; Maeda, K. Supramolecular Helical Systems: Helical Assemblies of Small Molecules, Foldamers, and Polymers with Chiral Amplification and Their Functions. *Chem. Rev.* **2016**, *116*, 13752–13990.

(106) Yashima, E.; Matsushima, T.; Okamoto, Y. Poly((4-carboxyphenyl)acetylene) as a Probe for Chirality Assignment of Amines by Circular Dichroism. *J. Am. Chem. Soc.* **1995**, *117*, 11596–11597.

(107) Fang, J.-M.; Selvi, S.; Liao, J.-H.; Slanina, Z.; Chen, C.-T.; Chou, P.-T. Fluorescent and Circular Dichroic Detection of Monosaccharides by Molecular Sensors: Bis[(Pyrrolyl)ethynyl]naphthyridine and Bis[(Indolyl)ethynyl]naphthyridine. *J. Am. Chem. Soc.* **2004**, *126*, 3559–3566.

(108) Ito, S.; Hiroto, S.; Ousaka, N.; Yashima, E.; Shinokubo, H. Control of Conformation and Chirality of Nonplanar π-Conjugated Diporphyrins Using Substituents and Axial Ligands. *Chem.-Asian J.* **2016**, *11*, 936–942.

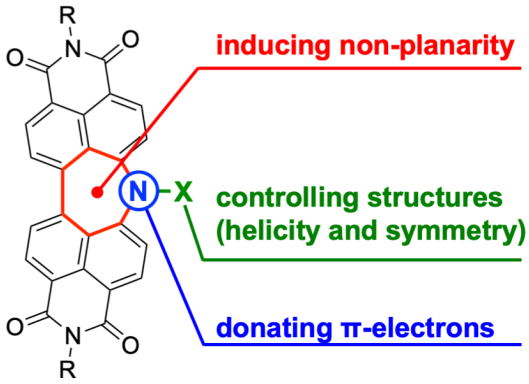
R
N
O
O
N
X
O
O
N
R
inducing non-planarity
controlling structures
(helicity and symmetry)
donating π-electrons